Journal of Sound and Vibration 330 (2011) 49–60

Contents lists available at ScienceDirect

Journal of Sound and Vibration

journal homepage: www.elsevier.com/locate/jsvi

Structural vibration control by synchronized switch damping energy transfer

Kaixiang Li*, Jean-Yves Gauthier, Daniel Guyomar

Université de Lyon, INSA-Lyon, LGEF EA 682, F-69621, Villeurbanne, France

ARTICLE INFO

Article history:
Received 25 March 2010
Received in revised form
28 June 2010
Accepted 23 July 2010
Handling Editor: D.J. Wagg
Available online 9 September 2010

ABSTRACT

The synchronized switch damping (SSD) technique has been demonstrated as an efficient means of suppressing structure vibrations. This paper presents a novel SSD technique based on an energy transfer (SSDET) scheme that transmits energy from an energy-source structure to a target structure in order to damp the latter. As a matter of fact, the transferred energy enhanced the synchronized switch damping on inductor (SSDI) with an initial current, thus leading to a better vibration control capability. The experiment, performed on a beam/plate system, succeeded in delivering an enhanced damping effect as compared to the SSDI technique by adopting the proposed control law. Comparisons between simulation and experiment also confirmed the effectiveness of the proposed mathematical model. The stability was discussed in order to determine the stability limit.

1. Introduction

Structural vibration control is a permanent issue in mechanical systems. A facile way of decreasing the vibrations is to strengthen the structure itself. However, this increases its weight, which can be fatal to certain structures with weight restrictions. Moreover, such an approach does not lead to the dissipation of the mechanical energy but rather transfers it to a higher mode motion.

During recent years, researchers have focused on using piezoelectric elements to damp structures. By connecting an optimized electrical impedance between piezoelectric elements, which are bonded to or embedded in the structure, an obvious damping effect has been observed when the structure vibrates around its natural frequency [1]. In a review article, Lesieutre reported on four basic shunt circuits, i.e., inductive, resistive, capacitive and switched circuits, and each shunt circuit could give rise to a different mechanical behavior [2]. Due to its simplicity and low power cost, the RL (resistor-inductor) circuit is one of the most researched and it shunts the terminals of piezoelectric elements with serial or parallel resistors and inductors. The oscillation frequency of this circuit is well tuned to the structural eigenvalue frequency in order to get a maximum damping effect [3]. The shortcomings of this technique include its high sensitivity to structure resonant frequency drift and the huge inductance requirement for low frequency control [4].

The switched shunt circuit has also received much attention during the last decade. Clark proposed the 'State Switching' technique in which piezoelectric elements play the role of a variable stiffness actuator. A simple control law is employed to switch the piezoelectric element between high and low stiffness in order to dissipate the vibration energy [5]. As key parameters in a switched shunt circuit, the timing and duration of the switching have also been investigated. It is pointed out that the optimal timing should be at the peak of the vibration cycle for closing and the peak of the next electrical cycle

* Corresponding author. Tel.: +33 472436210; fax: +33 472438874.
E-mail addresses: kaixiang.li@insa-lyon.fr (K. Li), jean-yves.gauthier@insa-lyon.fr (J.-Y. Gauthier), daniel.guyomar@insa-lyon.fr (D. Guyomar).

0022-460X/$ - see front matter © 2010 Elsevier Ltd. All rights reserved.
doi:10.1016/j.jsv.2010.07.021

for reopening [6]. In order to overcome the changes of external excitation or structure, Davis proposed a "ladder" capacitive shunt circuit so as to track such alterations and re-tune the circuit by connecting an appropriate capacitance [7].

More recently, a nonlinear vibration control method, called the synchronized switch damping (SSD) technique, has been developed [8,9]. This approach involves the switch being closed intermittently when the voltage of the piezoelectric elements reaches an extreme value. This leads to a time lag between the piezoelectric strain and the resulting voltage, and thus to a dissipation of energy. Some typical networks have been developed, including synchronized switch damping on short circuit (SSDS) [10], synchronized switch damping on inductor (SSDI) [11,12] and synchronized switch damping on voltage (SSDV) source [13–15]. These techniques exhibit a decent robustness against environmental drifts and broadband frequency control, all the while requiring only small amounts of external energy. Moreover, a self-powered and wireless vibration SSDI control scheme has already been achieved without any bulky electronic device or external computer [16].

The present paper introduces a novel SSD vibration control approach that enhances the SSDI by transferring the energy from another vibrating structure. The transferred energy increases the inversion factor of the SSDI on the target structure, thus leading to an improved damping effect as opposed to the classic SSDI technique. Results from simulation and experiment validate its effectiveness. Particularly, the provided energy does not originate from a traditional energy source, such as a battery, but rather from a vibrating structure.

The organization of the paper is as follows. Section 2 presents the principle of the classic SSDI and the proposed SSDET technique, and gives a comparison of the current and voltage of these two approaches during the switching instant. Section 3 aims at confirming the SSDET on a beam/plate system and Section 4 depicts the mathematical model under state space, which exposes the changes in the mathematical representation during the switching duration. Section 5 compares the simulation results with the experimental data so as to validate the proposed model and Section 6 discusses the control stability of the SSDET with regard to both experiment and simulation. Finally, Section 7 briefly concludes the paper.

2. Principles

This section presents the principles of the classic SSDI and the proposed SSDET techniques. The comparisons between SSDI and SSDET in current and voltage during the switching duration have demonstrated an improvement of the SSDET upon increasing the inverted voltage of the piezoelectric elements.

2.1. SSDI principles

The structure coupled with piezoelectric elements is often described by a model with a single degree of freedom as shown in Fig. 1. Here, m is the structure mass, c is the damping coefficient and k^E is the short-circuit stiffness. Furthermore, f is an external force exerting on the structure, C_0 is the natural capacitance of the piezoelectric elements on the structure, u is the displacement of the structure and V is the voltage between two electrodes of the piezoelectric element. This electromechanical coupling system can generally be formulated according to (1):

$$\begin{cases} m\ddot{u}+c\dot{u}+k^E u = f-\alpha V \\ i = \alpha\dot{u}-C_0\dot{V} \end{cases} \tag{1}$$

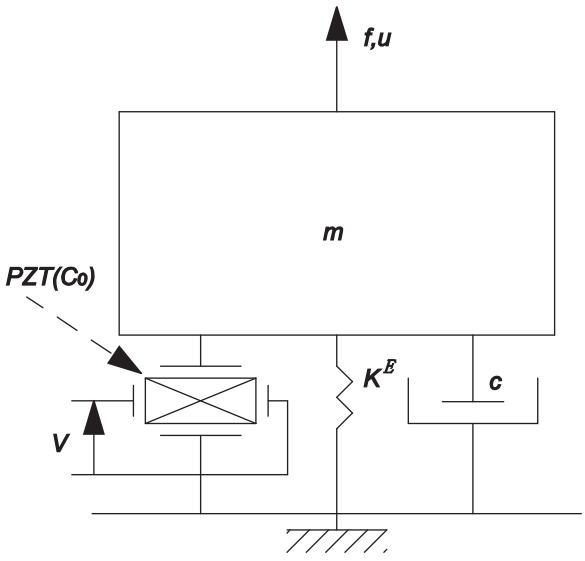

Fig. 1. An electromechanical model.

Here, i is the outgoing current from the piezoelectric elements and α is the force factor related to the piezoelectric material. The classical SSDI circuit consists of an inductor L, a resistor R and a pulse switch SW, which are connected to the piezoelectric elements, thus composing a simple LCR circuit as presented in Fig. 2. When the SW switch is closed, the voltage on the piezoelectric elements C_0 yields

$$V = L\frac{di}{dt} + Ri \tag{2}$$

The principle of the SSDI technique can be described according to the following: when the sensor detects the extremes of the displacement, a control device generates a timing pulse to close the switch, with the pulse width equaling the half period of the circuit. In this duration, the voltage on the piezoelectric elements becomes inverted. Due to the energy loss in the circuit, the absolute value of the inverted voltage V_m is consistently below V_M. The relationship between the voltage before inversion V_M and after inversion V_m is given in Fig. 3. The inversion factor γ can be calculated by an electric quality factor Q_i according to (3), and the vibration suppression coefficient η can be calculated according to (4):

$$\gamma = e^{-\pi/(2Q_i)} = \frac{V_m}{V_M} \tag{3}$$

$$\eta = \frac{1}{1+(4/\pi(1+\gamma/1-\gamma))k_{31}^2 Q_M} \tag{4}$$

Here, k_{31} is the electromechanical coupling coefficient (assuming the poling direction is perpendicular to the structure surface) and Q_M is the quality factor of the mechanical system [17]. It is clearly shown that the dissipated energy depends on γ, k_{31} and Q_M. Since k_{31} and Q_M are determined by the piezoelectric material property and the host structure and cannot be easily changed once they have been chosen, the only way to enhance the damping is to increase the inversion factor γ. The latter method represents such an attempt to increase γ artificially with an additional power supply.

2.2. SSDET principles

Due to it differing from most of the published vibration control techniques, the proposed method involves a variety of vibrating structures. One of them is the target structure, for which the vibration needs to be attenuated, and another structure (here referred to as the energy-source structure) is used to transfer its mechanical energy to the target structure by an electrical circuit aiming at a better damping effect to the target structure. In fact, the SSDET is similar to the classic SSDV technique since they both enhance the damping effect by an external source. The difference is that the energy source of SSDET is not a man-made voltage like SSDV but another structure, and may even be the target structure itself.

The ideal SSDET control scheme is described in Fig. 4. It consists of two LCR circuits sharing an inductor L and a resistor R. C and V are the capacitance of and the voltage on the piezoelectric elements, respectively. The subscripts *es* and *ts*, respectively, indicate the variables related to the energy-source structure and the target structure. The two switches are in the opened state most of the time and only need to be switched on when the voltage, the image of the displacement, reaches either a maximum or a minimum value. The corresponding operations could be carried out in the two following steps:

- *Step* 1: When the target structure vibration reaches its extreme displacement, SW_{es} is switched on till V_{es} drops to zero. In other words, the current i increases to its first extreme, and then SW_{es} is switched off. During this period, the electrical energy that has been converted from energy-source mechanical energy is stored in the inductor. This process is shown in the right part of Fig. 4, which could be called as an energy storing process.

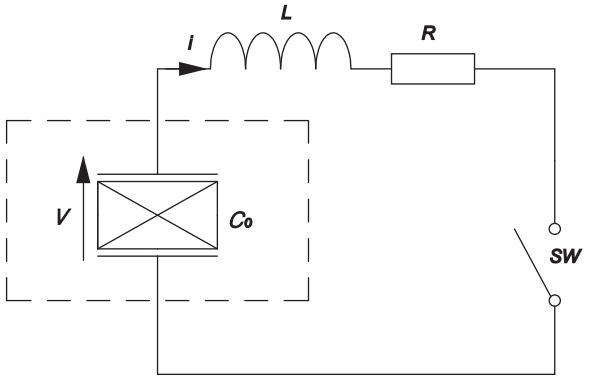

Fig. 2. A classic SSDI circuit.

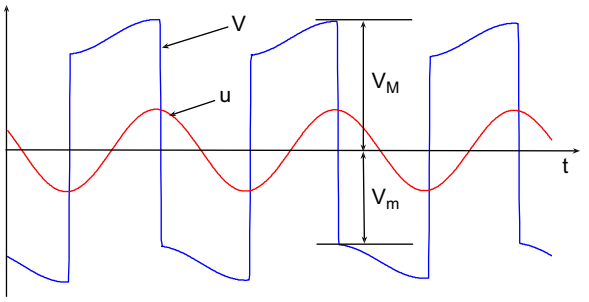

Fig. 3. The displacement and voltage typical waveforms of SSDI.

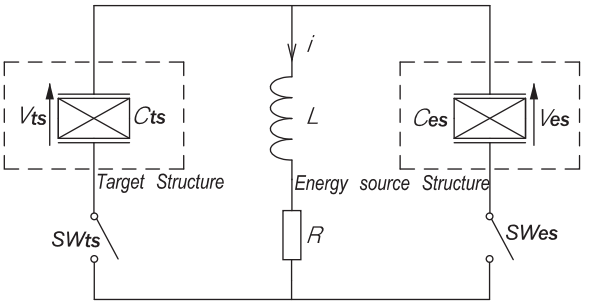

Fig. 4. The SSDET electrical circuit.

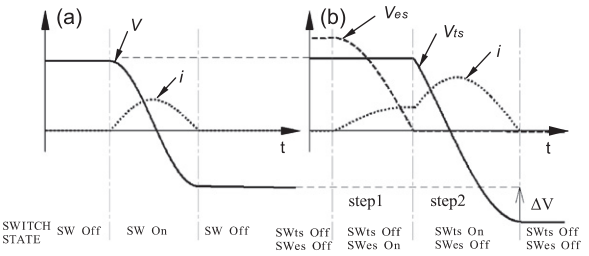

Fig. 5. Comparisons between the SSDET and SSDI techniques: (a) SSDI waveforms and (b) SSDET waveforms.

- *Step* 2: Considering that the LCR resonant frequency is much higher than the structure vibration frequency, step 1 could be implemented in a very short time while the displacement of the target structure u_{ts} would be maintained around its extreme during this period. When SW_{es} is re-opened, SW_{ts} is immediately switched on till V_{ts} is inverted. Subsequently, SW_{ts} is opened again. This process is shown in the left part of Fig. 4 and can be referred to as an energy transferring process.

Fig. 5 exposes the waveforms of the SSDI and the SSDET techniques during the closing of the switches. For the classical SSDI method, the piezoelectric voltage is simply inverted during half of the circuit period. The current i increases when the voltage V decreases. It reaches a maximum when V drops to zero and then decreases till V is inverted to its opposite extreme. As compared to the SSDI technique, the proposed SSDET method contains two inversions. In the first inversion, V_{es} is not totally inverted but cutoff at zero. The operation in step 2 is the same with SSDI but begins with an initial inductor current, thus giving rise to a greater inversion. Due to the initial current, the inversion factor could be even larger than one. In the SSD technique, it is known that the energy dissipation depends in particular on the voltage inversion factor. Hence, the proposed method was able to show a better damping performance as opposed to the SSDI control technique, and did not require any specific external power supply but rather only other vibration objects. From the point of view of the energy-source structure, it was also possible to damp its vibration since the mechanical energy was partially scavenged out of it.

The signs of V_{es} and V_{ts} could be either the same or opposite at the beginning of step 1, which determines different switch-closing durations. If the signs of V_{es} and V_{ts} are the same, SW_{es} should be closed for a quarter of an oscillation period, which roughly equals to $\sqrt{LC_{es}}$ in the energy storing process (assuming that the resistance is small). Otherwise, the SW_{es} should be closed for a longer time to make sure that the sign of the voltage on the inductor was the same as for V_{ts} at the

end of step 1. By doing so, the energy stored in the inductor consistently enhanced the voltage inversion in step 2. Due to it being different from t_1, the switching duration t_2 in step 2 was not constant but depended on the initial conditions. Based on the second-order circuit relations, the switch-closing duration in each step, i.e., the control law, can be summarized as follows:

$$\begin{cases} t_1 = \dfrac{1}{\omega_0}\arctan\left(\dfrac{\omega_0}{\xi}\right) & t_2 = \dfrac{1}{\omega_1}\left[\arctan\left(\dfrac{-i_0\omega_1 L}{U_0 - i_0\xi L}\right)+\pi\right] \quad \text{sign}(V_{es})\,\text{sign}(V_{ts}) \geq 0 \\ t'_1 = \dfrac{1}{\omega_0}\left[\arctan\left(\dfrac{\omega_0}{\xi}\right)+\pi\right] & t'_2 = \dfrac{1}{\omega_1}\left[\arctan\left(\dfrac{-i_0\omega_1 L}{U_0 - i_0\xi L}\right)+\pi\right] \quad \text{sign}(V_{es})\,\text{sign}(V_{ts}) < 0 \end{cases} \tag{5}$$

Here, $\xi = R/2L$. U_0 and i_0 are the initial voltage of the V_{ts} and the initial current in the inductor at the beginning of step 2, ω_0 and ω_1 are the resonant circular frequency of the energy storing circuit and the energy transferring circuit. These parameters can be obtained from Eq. (6). It should be pointed out that t_1 and t'_1 are always constant since they are only determined by the L, C and R properties. Nevertheless, t_2 and t'_2 are variable due to the different initial conditions of step 2 (U_0 and i_0) for each transfer time:

$$\omega = \sqrt{\frac{1}{LC} - \left(\frac{R}{2L}\right)^2} \tag{6}$$

One should note that the V_{ts} cannot be zero at its extreme value. However, it could still have the possibility that the V_{es} just equals to zero at the closing instant. In this case, the energy-source structure cannot supply any energy for the target structure, thus there would be no current in step 1. Therefore, a pure SSDI will be conducted on the target structure without initial current. The corresponding control strategy could be chosen as an alternative one from Eq. (5). As known, a time delay (t_1 or t'_1) exists between the displacement extreme instant of the target structure and the closing instant of SW_{ts}. Considering the first expression of Eq. (5) could give rise to shorter delay ($t_1 < t'_1$); the closing instant is more close to these extremes, leading to a better SSDI.

3. Experiment

This section presents the experiment performed to validate the SSDET technique by means of transferring energy from a cantilever beam to a four-edge clamped plate in order to suppress the motion of the plate.

3.1. Experimental setup

The schematic diagram of the experiment is shown in Fig. 6(a). The energy-source structure was the cantilever beam clamped on a rigid structure, and the target structure was a four-edge clamped plate. Both of the two structures were made of steel. Eight piezoelectric patches (PZT) were bonded at the root of the beam with a parallel connection and their equivalent capacitance was 44.5 nF. A commercial piezoelectric patch (ACX Quickpack QP10N, PZT) with a capacitance of 44.2 nF was bonded on the plate near the clamped edge in order to receive the transferred energy and damp the plate. The poling direction of all the piezoelements was perpendicular to the structure surface. The electrical circuit was simply composed of two switches (dual-MOSFETs with diodes) and a tunable inductor. The displacement of the plate was measured at its geometric center by an inductive proximity sensor. The geometric characteristics of the structures and piezoelectric elements are summarized in Table 1.

The structures were driven by an electromagnet under their first-mode natural frequencies, which were 22.3 Hz for the beam and 50.7 Hz for the plate. A dSPACE system was used to control the switches and store the sensed signatures.

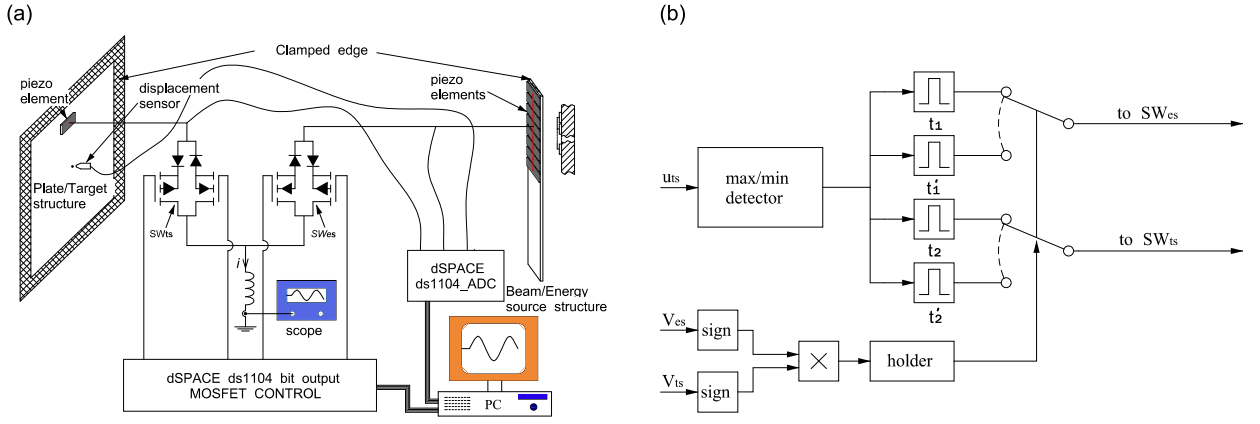

Fig. 6. A schematic diagram of the experiment: (a) the experimental setup and (b) the switching control scheme.

Table 1
Geometric characteristics.

	Length (mm)	Width (mm)	Thickness (mm)
Beam	345	4.00	2.50
Plate	400	300	0.5
PZT on beam	40.0	20.0	1.00
PZT on plate	50.0	25.0	0.37

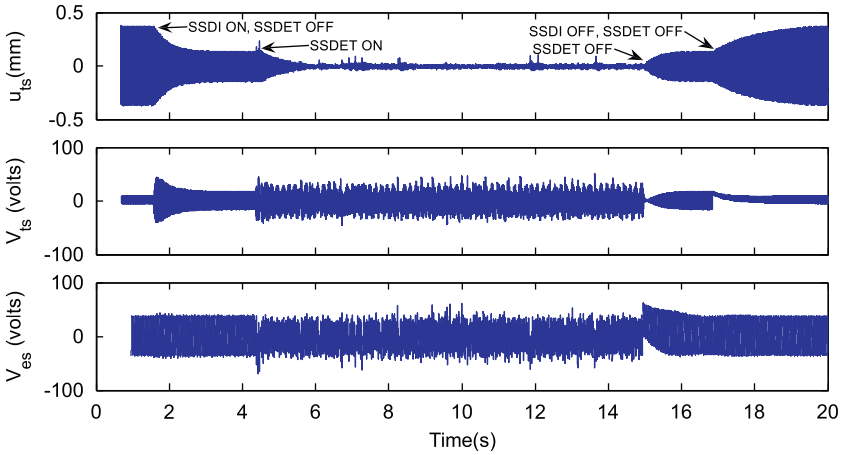

Fig. 7. The damping of the plate by SSDI and SSDET.

The switching control platform was developed by the simulink/dSPACE system, as shown in Fig. 6(b), to detect the extremes of the plate displacement and generate a timing pulse to control the switches. From the control law (5), the signs of piezoelectric voltage led to two switching strategies, and it was thus necessary to detect the voltage sign of the piezoelectric patches simultaneously on both the beam and plate to determine which strategy should be implemented. It should be pointed out that the switching strategy was only determined by the sign relationship between V_{ts} and V_{es} at the very beginning of step 1, and it should not be changed during the whole switching period. Thus, a holder was designed in the control system to hold the sign judgment during one switching period (both steps 1 and 2) to avoid any misestimating due to the voltage sign changing.

The switching duration t_1 in step 1 could be precisely set since it was constant and equals to 1/4 (voltages with same sign) or 3/4 (voltages with different signs) circuit period. However, t_2 was difficult to set accurately since it was a function of the initial voltage of the PZT on the plate and the current of the inductor as shown in Eq. (5). Detecting a precise current value is not possible since it needs an extremely fine step size in the control system, leading to a heavy memory space. Moreover, the noise in the current generated during the switching instant could easily result in false current detection. Fortunately, the current direction cannot be changed, even when the switching time is larger than the precise time t_2 or t'_2 in Eq. (5). Since the diode in the switch can stop the current from another direction, this could ensure the holding of the voltage at its extremes for a certain period of time after the current drops to zero. In practice, the switching duration for SW_{es} was set to the half period of the $RC_{es}L$ circuit, which is always larger than t_2.

3.2. Experimental results

Fig. 7 shows the damping effect of the plate by both the SSDI and SSDET techniques. The experiment demonstrated that the SSDET method gave rise to a better damping effect than the SSDI technique. At first, both structures vibrated under their first mode. The SSDI performed from 1.7 s, and the plate vibration consequently decreased in this period. When the vibration of the plate reached the stable state at 4.7 s, the SSDET approach performed the energy transfer from the vibrating beam to the piezoelectric patch on the plate and enhanced the damping effect. From 15.4 s, the SSDET was stopped and only the SSDI remained active. Finally, all the controls were stopped and the amplitude of the beam returned back to its original value after 16.8 s.

As discussed in Section 2, the signs of the piezoelectric initial voltage on the beam and plate have two possibilities, which lead to four different current waveforms as shown in Fig. 8. Under the proposed control law, the sign of V_{es} is the same as for V_{ts} at the closing instant of switch SW_{ts}. Thus, the transfer energy always enhances the current and leads to a large inversion of the voltage. Due to the phase difference between the two structures, the current intensity is not the same

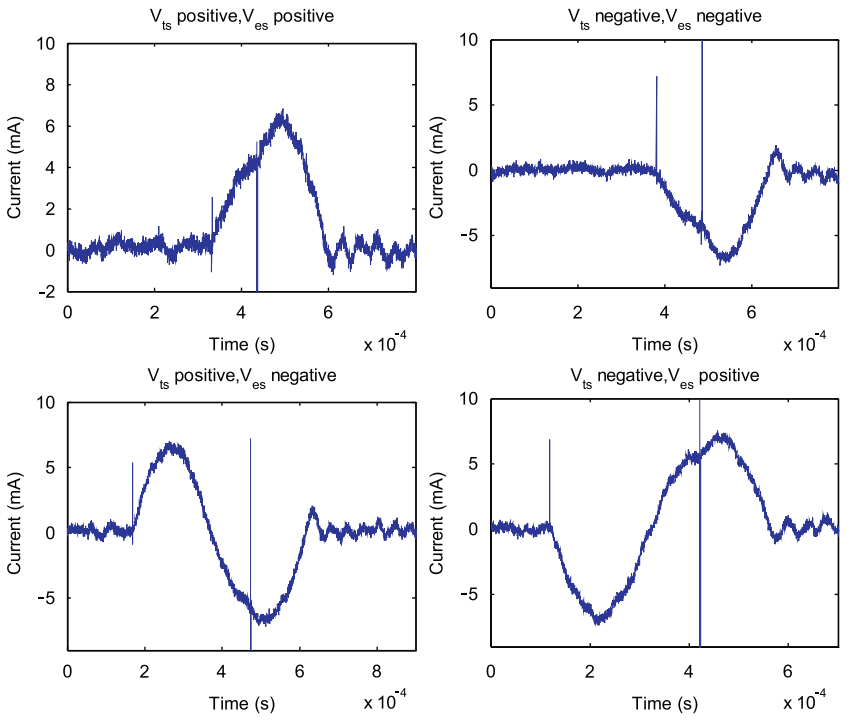

Fig. 8. Typical waveforms of the current when the switches were closed.

in each transfer. In other words, a larger displacement of the energy-source structure indicates a greater transferred energy at the transfer instant. One may observe that the current always jumps to a high level in a very short time and then returns back to its primary value at each switch-closing instant. This could be the contribution of the tiny parasitic capacitance in the circuit, which would be charged in each closing moment, thus inducing such jitter. Furthermore, the parasitic capacitance does not cause the circuit to completely open even though all switches are opened, which explains the current fluctuation around zero after step 2. Such a fluctuation could cause the electrical energy to dissipate, thereby decreasing the damping effect.

4. Mathematical model of the SSDET

This section proposes an electromechanical coupling equation for SSDET by employing a state space representation. Since the SSDET circuit consists of two separate LCR oscillators, the equations of SSDI can also be adopted for each step of the SSDET technique. Combined with Eqs. (1)–(3), the governing equation is represented in terms of a state space formulation:

$$\dot{\mathbf{x}}(t) = \mathbf{A}\mathbf{x}(t) + \mathbf{B}\mathbf{f}(t) \tag{7}$$

Here, the state vector **x(t)** is chosen as

$$\mathbf{x}(t) = [u_{es}\dot{u}_{es}u_{ts}\dot{u}_{ts}v_{es}v_{ts}i]^{T} \tag{8}$$

The state matrix **A** is a 7×7 matrix and can be divided into four blocks:

$$\mathbf{A} = \begin{bmatrix} \mathbf{A}_1 & \mathbf{A}_2 \\ \mathbf{A}_3 & \mathbf{A}_4 \end{bmatrix} \tag{9}$$

where

$$\mathbf{A}_1 = \begin{bmatrix} 0 & 1 & 0 & 0 \\ -k_{es}^E/m_{es} & -c_{es}/m_{es} & 0 & 0 \\ 0 & 0 & 0 & 1 \\ 0 & 0 & -k_{ts}^E/m_{ts} & -c_{ts}/m_{ts} \end{bmatrix} \tag{10}$$

$$\mathbf{A}_2 = \begin{bmatrix} 0 & 0 & 0 \\ -\alpha_{es}/m_{es} & 0 & 0 \\ 0 & 0 & 0 \\ 0 & -\alpha_{ts}/m_{ts} & 0 \end{bmatrix} \tag{11}$$

$$\mathbf{A}_3 = \begin{bmatrix} 0 & \alpha_{es}/c_{es} & 0 & 0 \\ 0 & 0 & 0 & \alpha_{ts}/c_{ts} \\ 0 & 0 & 0 & 0 \end{bmatrix} \tag{12}$$

$\mathbf{A}_1$ includes only the parameters of mass, damping and short circuit stiffness, and it thus represents the mechanical properties of the coupling system. $\mathbf{A}_2$ and $\mathbf{A}_3$ can be seen as electromechanical coupling matrixes which reveal the interaction between structures and piezoelectric elements. $\mathbf{A}_4$ shows the electrical properties of the system and it has different forms under varying control stages.

When both of the switches are open, the current i is zero and $\mathbf{A}_4$ can be written according to

$$\mathbf{A}_4 = \begin{bmatrix} 0 & 0 & 0 \\ 0 & 0 & 0 \\ 0 & 0 & 0 \end{bmatrix} \tag{13}$$

When SW_{es} is closed while SW_{ts} is open (step 1), $\mathbf{A}_4$ could be written as

$$\mathbf{A}_4 = \begin{bmatrix} 0 & 0 & -1/C_{es} \\ 0 & 0 & 0 \\ 1/L & 0 & -R/L \end{bmatrix} \tag{14}$$

When SW_{es} is open while SW_{ts} is closed (step 2), $\mathbf{A}_4$ can be written according to

$$\mathbf{A}_4 = \begin{bmatrix} 0 & 0 & 0 \\ 0 & 0 & -1/C_{ts} \\ 0 & 1/L & -R/L \end{bmatrix} \tag{15}$$

Considering two external forces $f_{es}(t)$ and $f_{ts}(t)$ exerted on each structure, the input vector $\mathbf{f}(t)$ can be written according to Eq. (16) and the input matrix $\mathbf{B}$ according to

$$\mathbf{f}(t) = [f_{es}(t) \quad f_{ts}(t)] \tag{16}$$

$$\mathbf{B} = \begin{bmatrix} 0 & 1/m_{es} & 0 & 0 & 0 & 0 & 0 \\ 0 & 0 & 0 & 1/m_{ts} & 0 & 0 & 0 \end{bmatrix}^{\mathrm{T}} \tag{17}$$

5. Numerical simulations

5.1. Model configurations and parameter identification

Numerical simulations were carried out on the beam/plate system, which was also adopted in the experiment. The diagram of the simulation model depicted in Fig. 9 was established in a Matlab/Simulink environment. Since the closing duration of step 2 was variable and due to the fact that there was no diode in the simulation, the system had to estimate the closing duration in step 2 according to the zero-crossing instant of the current. Once this zero-crossing instant was detected, the SW_{es} opened immediately. However, the derivative of the current around zero was large, and even a small delay would lead to a large deviation of the current from zero. Considering the tradeoff between the simulation efficiency

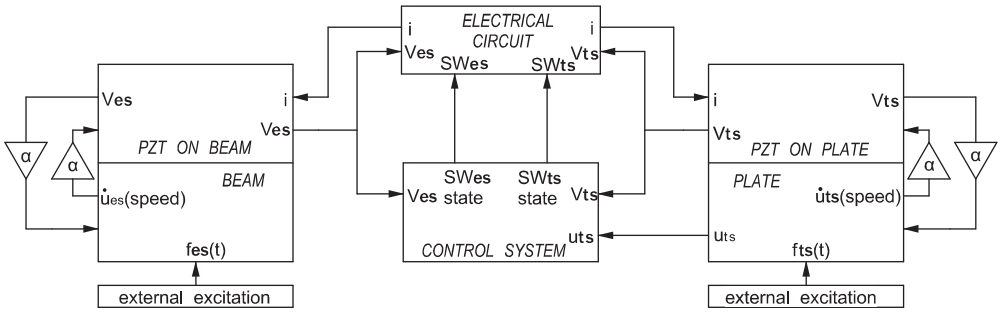

Fig. 9. A diagram of the simulation model.

and the accuracy, the time step size was set to 3×10^{-6} s, which was sufficient when compared to the oscillation period of the circuit (4×10^{-4} s for both oscillators).

The values of the system properties listed in Table 2 were identified from the vibration suppression experiment described in the previous section or calculated from Eqs. (18)–(22). The superscripts E and D stand for the piezoelectric elements being short-circuited and open-circuited, respectively. Considering the equivalent resistance of the coil, the piezoelectric patches and other losses in the circuit, the resistance was empirically determined to be 300 Ω. The mechanical quality factor Q_M was obtained from the half-power bandwidth method, where λ is the proportionality coefficient between voltage and displacement in open circuit, ω is the natural circular frequency of the structure, and ζ is the structural damping ratio. It should be pointed out that the values for the mass, stiffness and damping are those equivalents to their first mode:

$$\alpha = \lambda C \tag{18}$$

$$k^E = \alpha\lambda \frac{\omega^{E2}}{\omega^{D2} - \omega^{E2}} \tag{19}$$

$$m = \frac{k^E}{\omega^{E2}} \tag{20}$$

$$\zeta = \frac{1}{2Q_M} \tag{21}$$

$$c = 2\zeta m \omega_D \tag{22}$$

5.2. Comparison between simulation and experiment

The simulation and experimental results were compared in order to confirm the mathematical model. The procedure of the simulation was the same as that in the experiment. Fig. 10 shows the comparisons between the experiment and the simulation in various control stages. At first, two structures were subjected to a harmonic excitation at their resonance frequencies, as shown in Fig. 10(a). Subsequently, SSDI control was performed according to Fig. 10(b), and it was found that the simulation results coincided well with those of the experiment. During each closing instant, a tiny fluctuation of the piezoelectric voltage on the beam was observed in the experiment, as can be seen in the magnified image in Fig. 10(b). It was attributed to the parasitic capacitance. Finally, the SSDET control was conducted as demonstrated in Fig. 10(c). It was found that the voltage of the piezoelements on beam was consistently stopped around zero at the moment SW_{es} reopened (which was also when the current was at a maximum) and the voltage of the plate was consistently enhanced by the initial current during each transfer, both in experiment and in simulation. Consequently, the control strategy could be confirmed. It was also found that the damping was better in the simulation than that in the experiment. The voltages in simulation were larger than in experiment despite a trend that was similar to that of the experimental data. This was attributed to the max/min detector detecting a more precise extreme causing the inversion to occur at a higher voltage in the simulation as opposed to in the experiment.

Table 2
System properties.

Symbol	Value (unit)
L	0.09 H
R	300 Ω
C_{es}, C_{ts}	44.5 nF, 44.2 nF
ω_{es}^E,ω_{ts}^E	139.8 rad s^{-1}, 318.2 rad s^{-1}
ω_{es}^D,ω_{ts}^D	140.1 rad s^{-1}, 318.6 rad s^{-1}
m_{es}, m_{ts}	135.6 g, 98.7 g
k_{es}^E,k_{ts}^E	2650 N m^{-1}, 9998.2 N m^{-1}
c_{es}, c_{ts}	0.2584 N m^{-1} s^{-1}, 0.3017 N m^{-1} s^{-1}
λ_{es}, λ_{ts}	1.6×10^4 V m^{-1}, 2.1×10^4 V m^{-1}
α_{es}, α_{ts}	7.2×10^{-4} N V^{-1}, 9.4×10^{-4} N V^{-1}
Q_{es}, Q_{ts}	73.9, 103.7
ζ_{es}, ζ_{ts}	6.8×10^{-3}, 4.8×10^{-3}
t_1,t_2	9.3688×10^{-5} s, 1.8738×10^{-5} s
t_1',t_2'	2.9465×10^{-4} s, 1.8738×10^{-5} s

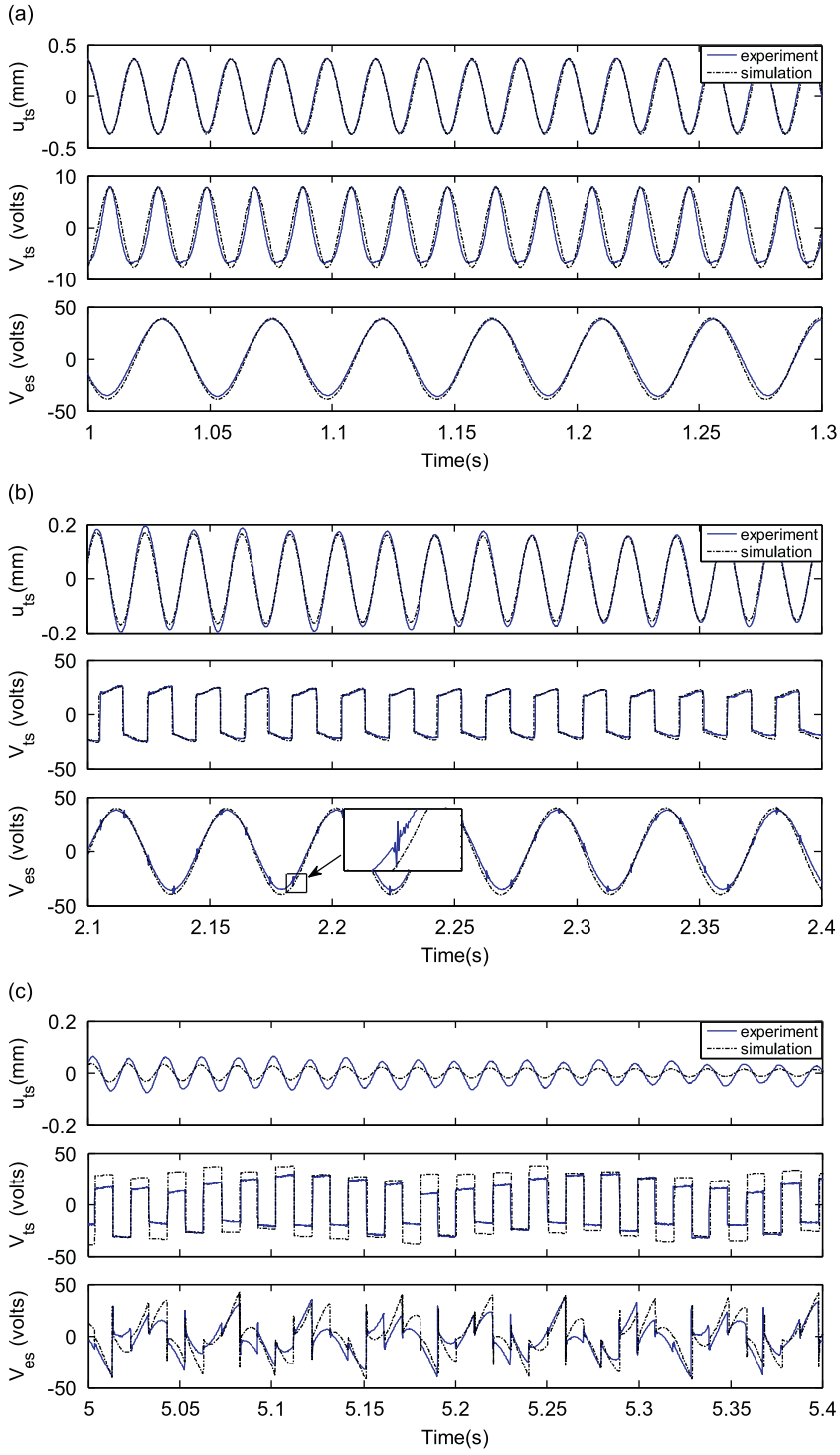

Fig. 10. A comparison between experiment and simulation: (a) without control, (b) with SSDI control and (c) with SSDET control.

6. Stability analysis

The stability of SSDET was confirmed both experimentally and through simulation. In this test, the plate was driven at its first natural frequency and was under the control of SSDI in the very beginning. The excitation of the beam was continuously increased until unstable control occurred on the plate. Fig. 11 shows the damping effect by SSDET beyond the

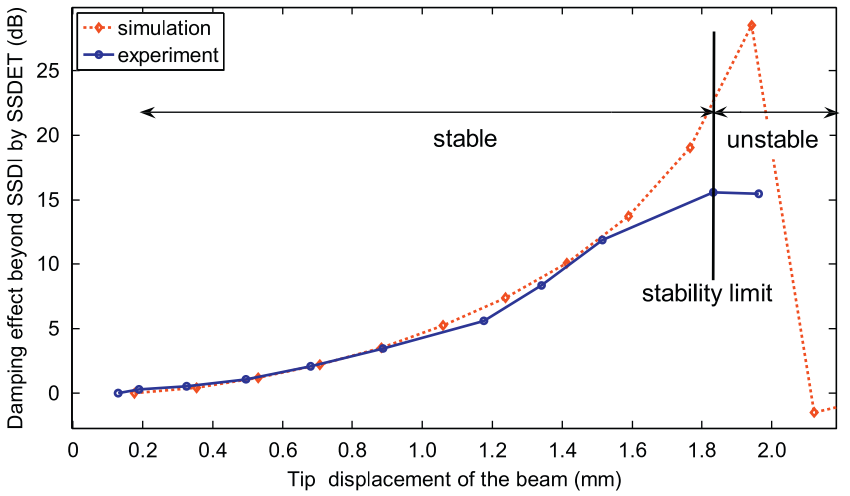

Fig. 11. The theoretical and experimental damping effect of SSDET beyond SSDI versus the displacement of the energy-source structure.

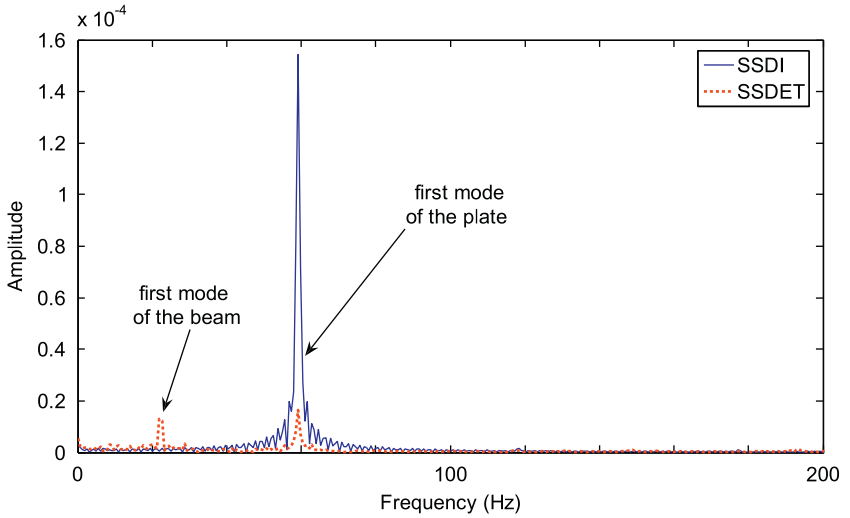

Fig. 12. A spectrum comparison between experimental SSDI and SSDET.

SSDI technique. The damping effect (y-axis) is defined as

$$\text{damping} = -20\log\frac{\delta_{\text{SSDET}}}{\delta_{\text{SSDI}}} \tag{23}$$

Here, δ is the root mean square of plate displacement.

It is clear that the damping effect increased with the beam displacement when this displacement was not too large. From the point of view of the transferred energy, it could be easily understood that more external energy was injected into the controlled structure, leading to a higher inverted voltage of the PZT patches on the plate, and thus to a better damping effect. Nevertheless, as a semi-active vibration control, the SSDET technique might generate instabilities. The damping effect was unable to increase monotonously when the beam vibrated with high amplitude. It was observed that the damping effect on the plate became destabilized for a tip displacement of the beam that was larger than 1.8 mm in the experiment, and it even sharply decreased in simulation. One reason was that the displacement of the plate became too attenuated and was no longer sinusoidal, especially in simulation, thus resulting in an erroneous switching timing. Moreover, the SSD technique, which sharply changes the stiffness of the structure, induces the residual modes, which also disturbs the max/min detector. This phenomenon could not be simulated by employing an SDOF model. In fact, even though the residual mode was not excited, the displacement of the plate would still be destabilized when its vibration is low while the transferred energy would remain high as in the classical SSDV control [18].

In order to reveal the frequency components of the plate displacement, the displacement of the plate from experiment under SSDI and SSDET control was transferred to the frequency domain presented in Fig. 12. The frequency component

under SSDI was mainly the excited frequency, i.e., the first-mode natural frequency of the plate. When SSDET was conducted, the first-mode frequency of the beam appeared in the plate motion, which signified that the vibration frequency of the energy-source structure could also affect the target structure while energy was being transferred. The experiment showed that the amplitude of this component was larger when the beam vibration level was higher, thus giving rise to a 'beating' phenomenon of plate displacement.

7. Conclusion

The proposed SSDET technique was found to broaden the SSD technique series. Although it belongs to the series of semi-active control, the external energy source was not a battery or a permanent voltage source but rather another vibration structure in order to achieve low energy consumption. Its damping capacity was demonstrated by the experiment carried out on a beam/plate structure. It should be pointed out that the two structures vibrated under different frequencies when energy was transferred, and the technique could thus be applied between any vibration structures. The mathematical model revealed that the system could be decomposed into three parts: a mechanical part, an electromechanical part and an electrical part, and that only the electrical part changed during each control stage. The comparison between simulation and experiment confirmed the effectiveness of the mathematical model. The stability analysis exposed that the sensed signal for judging the max/min moment would be disturbed by an excited high residual mode, especially when the structural vibration became too attenuated. It could also be destabilized when the energy-source structure vibration level was high while the target structure vibration level was low. As a result, future work should focus on developing an adaptive energy transferring scheme to avoid instabilities as the synchronized switching damping on the adaptive voltage source technique [19]. The energy transfer between multi-patches (i.e., more than two) should also be conducted between various structures or different locations in a single structure.

References

[1] N.W. Hagood, A. von Flotow, Damping of structural vibrations with piezoelectric material and passive electric networks, *Journal of Sound and Vibration* 146 (1991) 243–268.
[2] G.A. Lesieutre, Vibration damping and control using shunted piezoelectric materials, *The Shock and Vibration Digest* 30 (1998) 187–195.
[3] H. Sun, Z. Yang, K. Li, B. Li, J. Xie, D. Wu, L. Zhang, Vibration suppression of a hard disk driver actuator arm using piezoelectric shunt damping with a topology-optimized PZT transducer, *Smart Materials and Structures* 18 (2009) 065010.
[4] A.J. Fleming, S. Behrens, S.O.R. Moheimani, Reducing the inductance requirements of piezoelectric shunt damping systems, *Smart Materials and Structures* 12 (2003) 57–64.
[5] W.W. Clark, Vibration control with state-switched piezoelectric materials, *Journal of Intelligent Material Systems and Structures* 11 (2000) 263–271.
[6] W.W. Clark, J. Schoenly, Evaluation of performance indices for tuning the switch timing of pulse-switched piezoelectric shunts for vibration control, *Proceedings of SPIE Smart Structures and Materials Conference* 5760 (2005) 402–412.
[7] C.J. Davis, An actively tuned solid-state vibration absorber using capacitive shunting of piezoelectric stiffness, *Journal of Sound and Vibration* 232 (1999) 601–617.
[8] D. Guyomar, A. Badel, Nonlinear semi-passive multimodal vibration damping: an efficient probabilistic approach, *Journal of Sound and Vibration* 294 (2006) 249–268.
[9] D. Guyomar, A. Faiz, L. Petit, C. Richard, Wave reflection and transmission reduction using a piezoelectric semi-passive nonlinear technique, *Journal of the Acoustical Society of America* 119 (2006) 285–298.
[10] C. Richard, D. Guyomar, D. Audigier, G. Ching, Semi-passive damping using continuous switching of a piezoelectric device, *Proceeding of SPIE Smart Structure and Materials Conference* 3672 (1999) 104–113.
[11] C. Richard, D. Guyomar, D. Audigier, H. Bassaler, Enhanced semi-passive damping using continuous switching of a piezoelectric device on an inductor, *Proceeding of SPIE Smart Structure and Materials Conference* 399 (2000) 288–299.
[12] H. Ji, J. Qiu, K. Zhu, Y. Chen, A. Badel, Multi-modal vibration control using a synchronized switch based on a displacement switching threshold, *Smart Materials and Structures* 18 (2009) 035016.
[13] E. Lefeuvre, A. Badel, L. Petit, C. Richard, D. Guyomar, Semi-passive piezoelectric structural damping by synchronized switching on voltage sources, *Journal of Intelligent Material Systems and Structures* 17 (2006) 653–660.
[14] H. Ji, J. Qiu, A. Badel, K. Zhu, Semi-active vibration control of a composite beam using an adaptive SSDV approach, *Journal of Intelligent Material Systems and Structures* 20 (2009) 401–412.
[15] H. Ji, J. Qiu, A. Badel, Y. Chen, K. Zhu, Semi-active vibration control of a composite beam by adaptive synchronized switching on voltage sources based on LMS algorithm, *Journal of Intelligent Material Systems and Structures* 20 (2009) 939–947.
[16] M. Lallart, E. Lefeuvre, C. Richard, D. Guyomar, Self-powered circuit for broadband, multimodal piezoelectric vibration control, *Sensors and Actuators A: Physical Control* 143 (2008) 377–382.
[17] C. Magnet, C. Richard, D. Guyomar, Towards smart vibration control for printed circuit boards, *Journal of Vibration and Control* 13 (2007) 1761–1783.
[18] A. Badel, G. Sebald, D. Guyomar, M. Lallart, E. Lefeuvre, C. Richard, J. Qiu, Piezoelectric vibration control by synchronized switching on adaptive voltage sources: towards wideband semi-active damping, *Acoustical Society of America* 119 (2006) 2825–2851.
[19] M. Lallart, A. Badel, D. Guyomar, Nonlinear semi-active damping using constant or adaptive voltage sources: a stability analysis, *Journal of Intelligent Material Systems and Structures* 19 (2008) 1131–1141.